Journal of Materials Chemistry A

Unexpected electrochemical behavior of an anolyte redoxmer in flow battery electrolytes: solvating cations help to fight against the thermodynamic-kinetic dilemma

Journal:	*Journal of Materials Chemistry A*
Manuscript ID	TA-ART-02-2020-002214.R1
Article Type:	Paper
Date Submitted by the Author:	27-Mar-2020
Complete List of Authors:	ZHAO, YUYUE; Argonne National Laboratory, Yu, Zhou; Argonne National Laboratory Robertson, Lily ; Argonne National Laboratory Zhang, Jingjing; Argonne National Laboratory, Chemical Sciences and Engineering Shi, Zhangxing; Argonne National Laboratory Bheemireddy, Sambasiva ; Argonne National Laboratory Shkrob, Ilya; Argonne National Laboratory, Chemical Sciences and Engineering Z, Y; UIUC, Department of Nuclear, Plasma, and Radiological Engineering, Department of Materials Science and Engineering, Department of Electrical and Computer Engineering Li, Tao; Argonne National Laboratory Zhang, Zhengcheng; Argonne National Laboratory, Chemical Engineering Division Cheng, Lei; Argonne National Laboratory Zhang, Lu; Argonne National Laboratory

Unexpected electrochemical behavior of an anolyte redoxmer in flow battery electrolytes: solvating cations help to fight against the thermodynamic-kinetic dilemma

*Yuyue Zhao[1,2,+], Zhou Yu[1,3,+], Lily A. Robertson[1,2,4], Jingjing Zhang[1,2], Zhangxing Shi[1,2], Sambasiva Reddy Bheemireddy[1,2], Ilya A. Shkrob[1,2], Y Z [1,5,6,7,8], Tao Li[1,9,10], Zhengcheng Zhang[1,2], Lei Cheng[1,2 *], Lu Zhang[1,2 *]*

[1] *Joint Center for Energy Storage Research, Argonne National Laboratory, Argonne, IL 60439, United States*

[2] *Chemical Sciences and Engineering Division, Argonne National Laboratory, Argonne, Illinois, 60439, United States*

[3] *Material Science Division, Argonne National Laboratory, Argonne, Illinois, 60439, United States*

[4] *Department of Chemistry, University of Illinois at Urbana−Champaign, Urbana, Illinois 61801, United States*

[5] *Department of Nuclear, Plasma, and Radiological Engineering, University of Illinois at Urbana−Champaign, Urbana, Illinois 61801, United States*

[6] *Beckman Institute for Advanced Science and Technology, University of Illinois at Urbana−Champaign, Urbana, Illinois 61801, United States*

[7] *Department of Materials Science and Engineering, University of Illinois at Urbana−Champaign, Urbana, Illinois 61801, United States*

[8] *Department of Electrical and Computer Engineering, University of Illinois at Urbana−Champaign, Urbana, Illinois 61801, United States*

[9] *Department of Chemistry and Biochemistry, Northern Illinois University, DeKalb, Illinois 60115, United States*

[10] *X-ray Science Division, Advanced Photon Source, Argonne National Laboratory, Argonne, Illinois 60439, United States*

TOC graphic

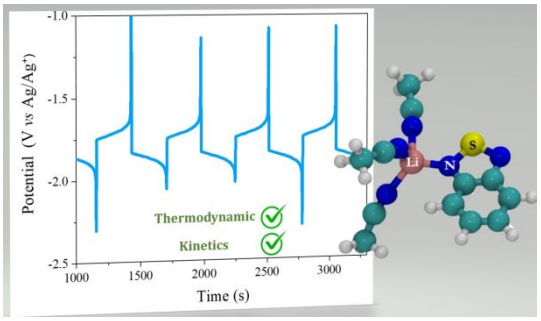

Keywords:

Nonaqueous flow battery, solvation interaction, 2, 1, 3-benzothiadiazole, redox potential, stability, redoxmer

Abstract

Redoxmers are redox-active molecules that can store energy in electrolytes for redox flow batteries (RFBs), and their electrochemical properties are significantly affected by the choice of supporting electrolytes. Herein, we use 2,1,3-benzothiadiazole (BzNSN) as a model system to scrutinize the supporting electrolyte impact. By systemically varying the components of supporting salts, BzNSN not only shows substantial redox potential shifts but also exhibits varying electrochemical stabilities. Specifically, changing the size of cations can effectively alter the coordination between the supporting salt and BzNSN species. From Li^+, Na^+, K^+, to NEt_4^+, the redox potential of BzNSN shifts negatively, from -1.63 V to -1.82 V vs Ag/Ag^+. Molecular Dynamics and Density Functional Theory simulations revealed that smaller cations, like Li^+, are closer to the charged BzNSN when coordinated, implying stronger coordination, while larger cations, like K^+ and NEt_4^+, are farther away. Interestingly, the large cation electrolytes also lead to much improved electrochemical stability, evidenced by the extraordinarily enhanced kinetic lifetime from electron paramagnetic resonance measurement. This study demonstrates the first example of tuning an anolyte redoxmer toward a concurrent improvement of lowered redox potentials AND enhanced calendar lives *via* solvation means, which is usually constrained by the thermodynamic-kinetic relation.

1. Introduction

Large-scale energy storage is a key component of the "smart grid" solution to addressing the intermittency challenge of renewable energy sources. Redox flow batteries (RFBs) are one of the most promising candidates for grid-scale stationary energy storage applications.[1-3] Unlike traditional batteries, whose energy densities are predetermined by the embedded solid electrodes, RFBs store electricity in the electrolyte solutions of redox-active materials. Depending on the materials used, these electrolytes afford various intrinsic redox potentials and circulate through the positive and negative electrode compartments for energy conversion. These species are denoted as catholyte and anolyte, respectively. The liquid nature of RFBs provides many unique features, including decoupled power and energy, ease of scale-up and low-cost optimization. [4-6] While much RFB progress focuses on aqueous electrolytes and some aqueous prototypes are becoming commercially available, such as vanadium and zinc-bromine RFBs, their energy densities are constrained by intrinsically low operating voltages (< 1.8 V) of water electrolysis reactions, which also contributes to high systematic cost.[7, 8] An attractive alternative to address this limitation is to develop nonaqueous RFBs (NRFBs) by taking advantage of the wider electrochemical windows of organic solvents (> 2 V). Numerous redox chemistries for NRFBs have been developed including inorganic active materials (sulfur and iodine species),[9, 10] redox-active polymers,[11, 12] and organometallic compounds [13, 14] as well as hybrid designs such as semi-solid[15, 16] and redox-targeting flow batteries, [17, 18] all attempting to harvest high energy densities. In particular, redox-active organic molecules (redoxmers) are attractive active materials. Those molecules are primarily constructed from organic aromatic systems that can be structurally modified with tunable properties, making them ideal candidates for NRFBs.[19-22]

As the most important component, the redoxmer-containing electrolytes often dictate the performance of NRFBs, and the redoxmers mostly determine the key parameters. In fact, engineering redoxmers towards certain redox potentials and high stability has been the most efficient approach for constructing high performance NRFBs. Higher potentials of catholyte redoxmers and lower potentials of anolyte redoxmers can lead to higher cell voltages and higher energy densities.[23] Although exceptions exist, redoxmers with better electrochemical stability (or calendar life) often result in improved cycling performance.[23-25] However, the choice of supporting electrolyte, i.e., the non-electroactive salt/solvent solution, also plays an important role. For instance, in our previous study, 2,1,3-benzothiadiazole (BzNSN), an energy-dense

anolyte molecule with a low redox potential (-1.58 V vs Ag/Ag^+) and high solubility (5.7 M in acetonitrile), showed stable cycling at high concentration in flow cells.[22, 23] During the investigation, we noticed that by changing the supporting salts, the redox potentials as well as the calendar life were dramatically impacted.[26] Similar phenomena have also been observed in other electrolyte systems. Another family of anolyte redoxmer, pyridinium-based derivatives, also showed shifted potentials and different cyclability in various supporting electrolytes.[27] In aqueous RFBs, the solvation structure of the concentrated aqueous TEMPO-based redoxmers correlates well with the cycling performance, which is due to the combined effects of the diffusivity and concentration of redoxmer and the ionic conductivity.[28] Moreover, adding chloride to a vanadium sulfate electrolyte can improve energy capacity and afford excellent electrochemical performance over a broader operation temperature window because of the formation of stable $VO_2Cl(H_2O)_2$.[29, 30] By blending iodide with bromide and/or chloride, zinc-iodine RFBs can achieve high capacity with long cyclic life. [31-33] The added halide ions act as a complexing agent to stabilize the iodine. Generally, understanding the solvation behavior of active materials in supporting electrolytes is of crucial importance to improve and optimize RFB performance. In this paper, we use BzNSN as a model system to scrutinize the supporting electrolyte impact on the electrochemical behavior.

2. Results and Discussion

A variety of electrolyte salts were chosen to investigate the effect of supporting electrolytes on the electrochemical behavior of BzNSN. Specifically, salt solutions of lithium bis(trifluoromethane)sulfonimide (LiTFSI), lithium hexafluorophosphate ($LiPF_6$), lithium bis(fluorosulfonyl)imide (LiFSI), sodium bis(trifluoromethane)sulfonimide (NaTFSI), potassium bis(trifluoromethane)sulfonimide (KTFSI), tetraethylammonium bis(trifluoromethane)sulfonimide (NEt_4TFSI), and tetraethylammonium hexafluorophosphate (NEt_4PF_6), were prepared in acetonitrile (CH_3CN), generally at 0.5 M, with some salts chosen for more extensive concentration studies.

Figure 1 shows the cyclic voltammograms of 10 mM BzNSN in Li^+ and NEt_4^+ supporting electrolytes as well as the half wave potential, $E_{1/2,}$ calculated by averaging the cathodic (E_{Pc}) and anodic (E_{Pa}) peak potentials. BzNSN maintains excellent redox reversibility in these electrolytes, but, as expected, the redox potentials are significantly affected. For electrolytes containing Li^+, $E_{1/2} \approx$ -1.6 V vs Ag/Ag^+, while the electrolytes containing the bulky NEt_4^+ are

much lower, with $E_{1/2} \approx$ -1.8 V vs Ag/Ag^+, an overall ~200 mV shift. Based on these data, the shift is attributed to the choice of cations as using different anions has minimal effect.

To further illustrate this effect, a mixed cation experiment was conducted using LiTFSI and NEt_4TFSI. Keeping the total overall concentration at 0.5 M, the salt ratio was varied from 0:0.5 to 0.1:0.4, 0.25:0.25, 0.4:0.1, and 0.5:0. As shown in Figure 2, increasing the ratio of LiTFSI in the electrolytes leads to increases of the measured redox potentials. From 0:0.5 to 0.1:0.4, a substantial shift (130 mV from -1.82 V to -1.69 V vs Ag/Ag^+) of the measured $E_{1/2}$ was observed. The increase becomes less significant with a further increase of the ratio of LiTFSI as from 0.1:0.4 to 0.5:0 only a shift of 60 mV (-1.69 V to -1.63 V vs Ag/Ag^+) was seen. The significant shift with a small addition of Li^+ implied that Li^+ may have much stronger interactions with BzNSN compared to NEt_4^+.

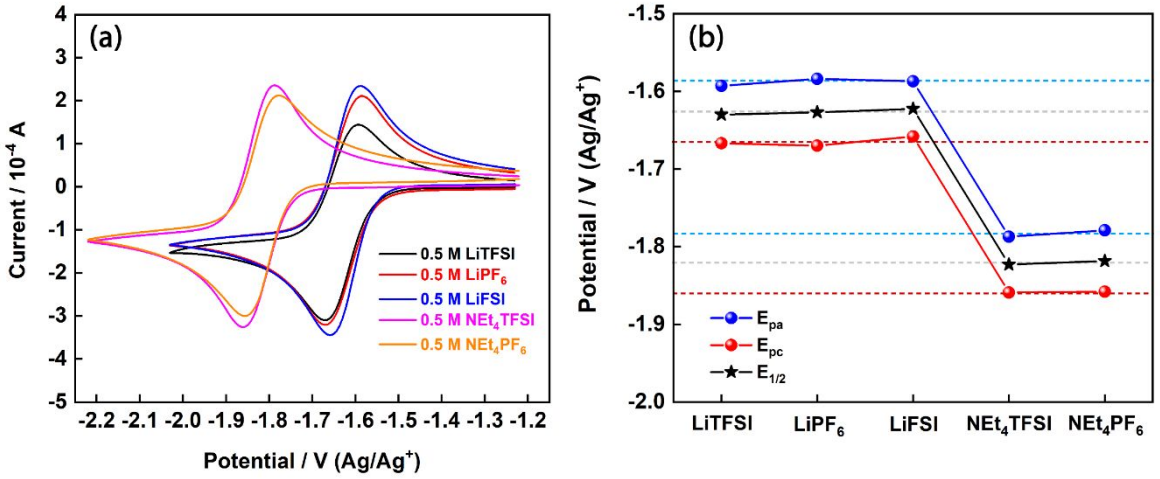

Figure 1. (a) Cyclic voltammograms and (b) corresponding redox potentials of BzNSN (10 mM) in various supporting electrolytes in CH_3CN (scan rate for all is 100 mV/s).

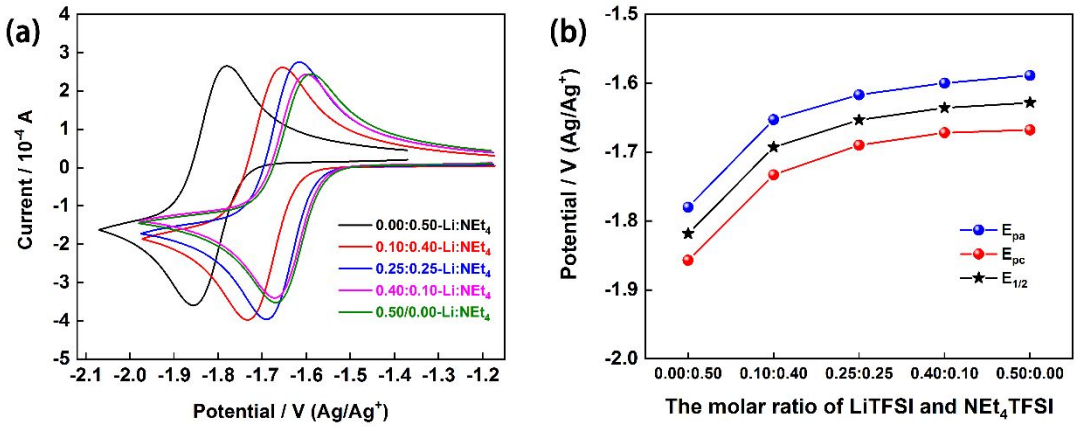

Figure 2. (a) Cyclic voltammograms and (b) corresponding redox potentials of BzNSN in various supporting electrolytes with different molar ratio of LiTFSI and NEt_4TFSI. The total concentration of LiTFSI and NEt_4TFSI is 0.5 M in CH_3CN, and the scan rate is 100 mV/s.

To further probe this cation effect, we examined a concentration series. We performed cyclic voltammetry of BzNSN in supporting electrolytes containing 0.1-1.0 M LiTFSI or NEt_4TFSI (Figure 3). For the LiTFSI series, the redox potential of BzNSN increased gradually as the salt increased, from -1.72 V at 0.1 M LiTFSI to -1.61 V at 1.0 M LiTFSI, ~110 mV shift. On the other hand, while the redox potentials of BzNSN in the NEt_4TFSI supporting electrolytes were much lower, they had little shift. A marginal increase (40 mV) was observed from -1.84 V at 0.1 M NEt_4TFSI to -1.80 V at 1.0 M NEt_4TFSI. The larger shift with the LiTFSI indicated that the concentration effect is stronger, supporting the hypothesis that Li^+ has stronger interactions with the BzNSN species.

Next, we chose to investigate the solvating interactions of other cations. As Li^+ and NEt_4^+ are very different in size, understanding the effect of cation radius on solvation was the next logical step. Thus, we chose Na^+ and K^+ as additional cations to systematically investigate the role of size. As shown in Figure 4, cyclic voltammetry of BzNSN solutions was conducted in supporting electrolytes using LiTFSI, NaTFSI, KTFSI, or NEt_4TFSI salts. As expected, the potentials of BzNSN exhibited a negative shift as the cations become larger. The $E_{1/2}$ of BzNSN decreased from -1.63 V in LiTFSI electrolyte to -1.77 V in NaTFSI electrolyte, demonstrating a 140 mV shift. From NaTFSI to KTFSI and NEt_4TFSI, the $E_{1/2}$ continued to decrease to -1.81 V and -1.82 V, but the shift (50 mV) was much smaller. The observed results support the idea that the strength of solvating interactions between cations and the BzNSN species are affected by cation size.

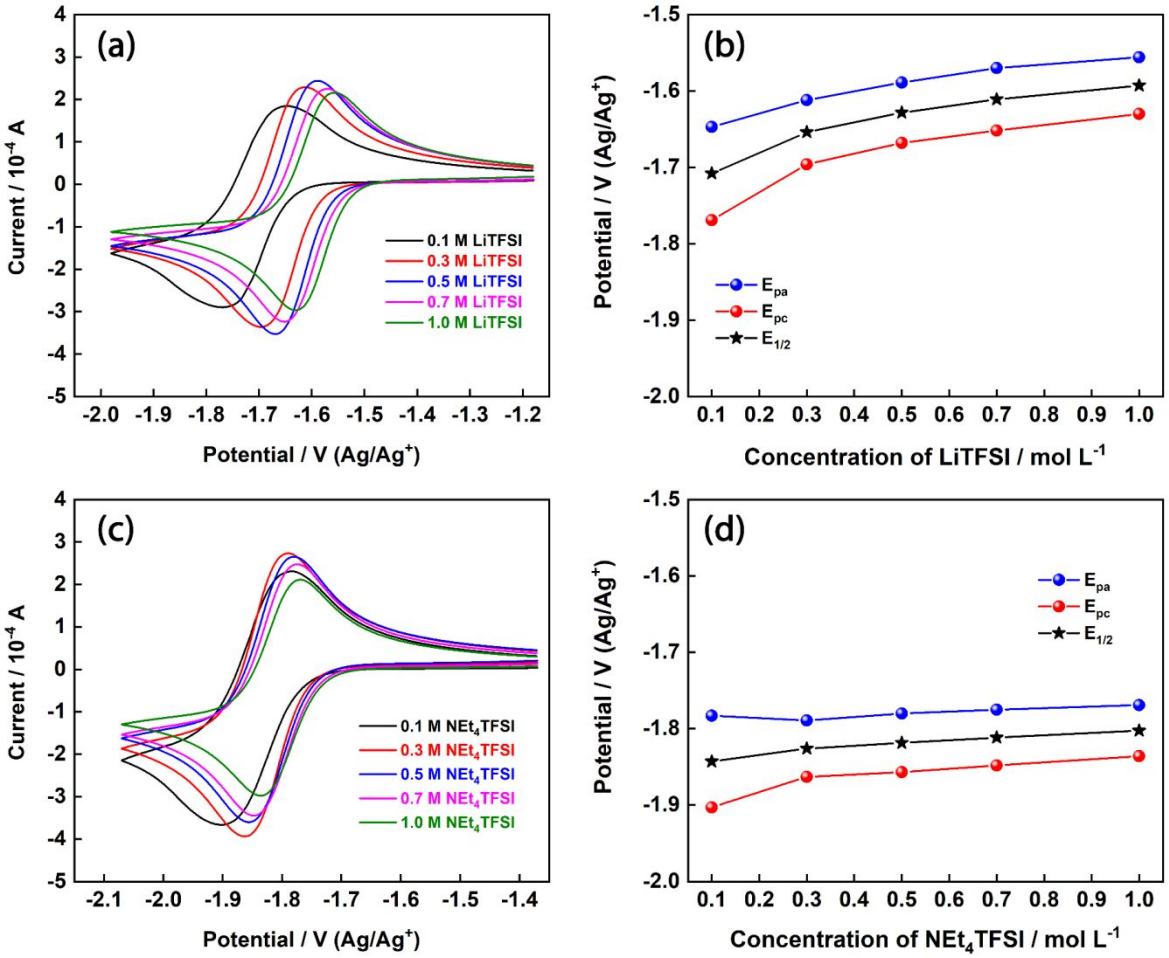

Figure 3. (a) Cyclic voltammograms and (b) corresponding redox potentials of BzNSN in supporting electrolytes with various concentrations of LiTFSI in CH_3CN; (c) cyclic voltammograms and (d) corresponding redox potentials of BzNSN in supporting electrolytes with various concentrations of NEt_4TFSI in CH_3CN. The concentration of BzNSN is 10 mM, and the scan rate is 100 mV/s.

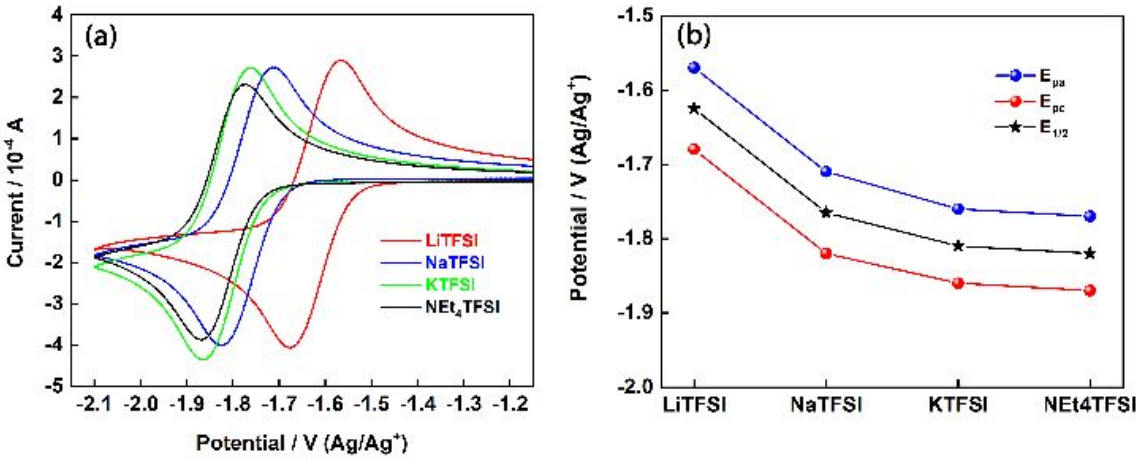

Figure 4. (a) Cyclic voltammograms of BzNSN and (b) corresponding redox potentials of BzNSN with different cations salts. The concentration of BzNSN is 10 mM in CH_3CN, the scan rate is 100 mV/s, and the anion is $TFSI^-$ in all cases.

To gain insight into these solvating interactions, theoretical simulations using molecular dynamic (MD) and density functional theory (DFT) were conducted. The details of the MD systems and DFT calculations can be found in the experimental section. The neutral and charged state of BzNSN were firstly investigated by characterizing their charge distributions. As shown in Figure 5a, the extra negative charge of the charged BzNSN (radical anion) has been distributed over the fused ring, resulting in large negative charges on nitrogen (N) atoms. On the other hand, while the neutral BzNSN also has negative charges on N atoms, the charge on the S atom is much more positive, which may hinder coordination with cations. Figure 5b1 summarizes the radial distribution function (RDF) from the N atom in the charged and neutral BzNSN to the cations (e.g., Li^+, Na^+, K^+, and NEt_4^+). The coordinates of NEt_4^+ are represented by the center N atom. The high intensity peaks in Figure 5b1 indicate strong coordination between the charged BzNSN and cations, while the intensity of those peaks in Figure S1a are much weaker, implying negligible coordination of neutral BzNSN. The peaks in Figure 5b1 also indicate the relative positions of corresponding cations. The longer distance and lower RDF means cations escape more easily from the charged BzNSN as the RDFs correlate to the Boltzmann distribution of the potential of mean force (PMF). [34] The first peaks of RDF are indicative of the closest cations to charged BzNSN, and the distance becomes larger with increased cation size. For instance, the distance between the N in BzNSN to Li^+ is ~2 Å, which increases to ~2.4 Å for Na^+, ~3.0 Å for K^+, and essentially ~5 Å for NEt_4^+. Meanwhile, for the Li^+, Na^+, and K^+, there are two clear peaks within 6 Å, indicating two cations coordinating with one charged BzNSN. This observation can be further illustrated in the coordination number plot. As shown in Figure 5b2, the first plateau occurs at a distance of 2~4 Å with a coordination number of ~1. When the distance increases to 4~6 Å, the second plateau appears, implying one more cation is involved in the coordination environment. There is no clear plateau for the NEt_4^+, implying a flexible and less defined solvation shell with the BzNSN species. This is to be expected due to the delocalized charge and non-coordinating nature of the NEt_4^+. A snapshot of representative solvation structure around charged BzNSN with the Li^+, Na^+, and K^+ salts is shown in Figure 5c. Specifically, two cations coordinate with the N atoms of the charged BzNSN. The solvation shells of the cations are further completed by solvent molecules (i.e., CH_3CN) and counterion (i.e., $TFSI^-$ ion). As the classical MD results can be sensitive to the

force fields, we also performed *ab initio* MD (AIMD) simulations to validate the solvation structures predicted by classical MD. From the trajectory (see the movie in the supporting information) we can see the same key coordination features seen from the classical MD simulations: the two cations bind with the N atoms of the charged BzNSN. The distance between Li^+ and the nitrogen of BzNSN is 2.05±0.09 Å in our AIMD simulation. These observations confirm the reliability of the force fields used in the classical MD simulation. As expected, contrary to the solvation shell features seen in Figure 5b for the charged BzNSN, there is no well-defined solvation between supporting salt cations and the neutral BzNSN as shown in Figure S1.

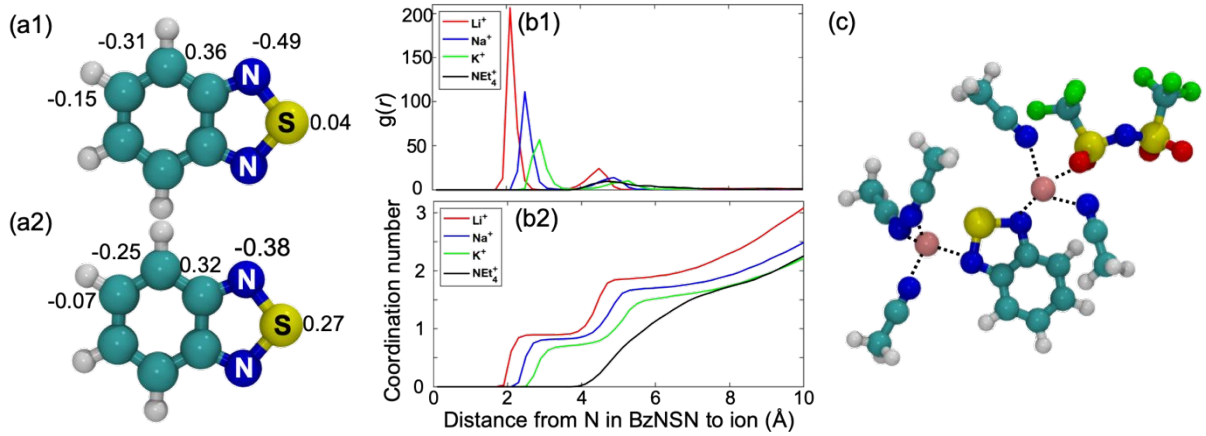

Figure 5. (a) Charge distribution of the charged (a1) and neutral (a2) BzNSN used in the force field. (b1) Radial distribution function (RDF) and (b2) coordination number of cations (e.g., Li^+, Na^+, K^+, and NEt_4^+) around the nitrogen atom in the charged BzNSN. The coordinates of NEt_4^+ are represented by the central nitrogen atom. (c) Representative solvation structure around the charged BzNSN with Li^+, Na^+, and K^+ salts. The pink, blue, yellow, cyan, white, red, and green ball denote cations (Li^+, Na^+, and K^+), N, S, C, H, O, and F atom.

The geometric structures of the charged BzNSN with various coordinated cations are optimized using DFT. As shown in Figure 6a, two cations are symmetrically coordinated with the charged redoxmer. While their relative positions are within a dynamic range (see Figure S2), the two cations generally share the same plane with the arene ring of BzNSN. As the cation size increases, they move farther from BzNSN (see Figure 6b), which is consistent with the results shown in Figure 5b. An approximate linear relationship exists between cation-N distance and the ionic radius. Redox potentials are also estimated based on the optimized structures, and the results are summarized in Table 1. The simulated redox potentials are consistent with the

experimental values. Since no clear solvation shell is observed for NEt_4^+ with the BzNSN species in the MD simulation, no redox potential can be estimated for BzNSN with NEt_4^+.

Table 1. Experimental (E-experiment) and calculated (E-simulation) redox potentials of BzNSN with various cations in CH_3CN.

	Li	Na	K
E-simulation (V)	-1.54	-1.74	-1.87
E-experiment (V)	-1.61	-1.76	-1.80

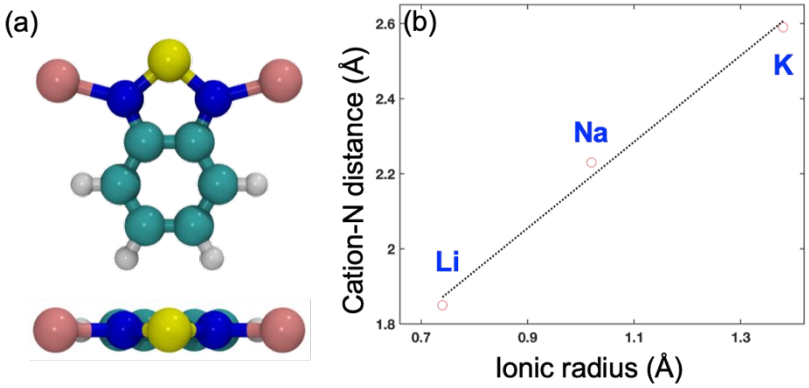

Figure 6. (a) Top and side view of the charged BzNSN with two coordinated cations. The pink, blue, yellow, cyan, and white ball denote cations (Li^+, Na^+, and K^+), and N, S, C, and H atom. (b) The distance between cation (Li^+, Na^+, and K^+) and N atom in charged BzNSN using DFT calculation with CPCM solvation model as a function of the ionic radius.

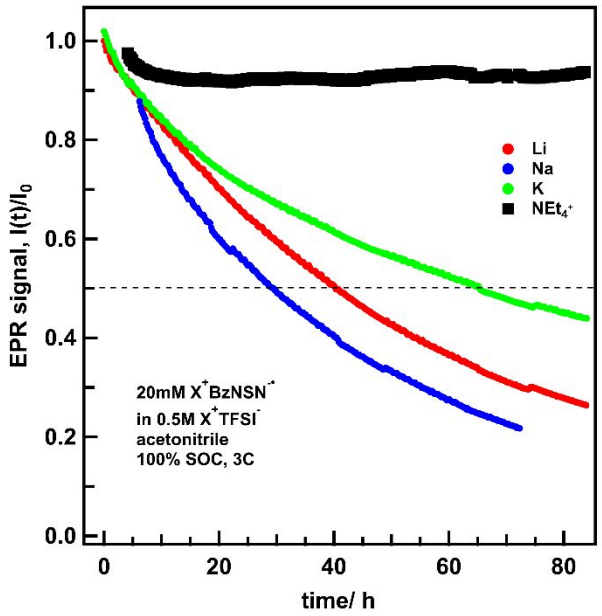

Figure 7. Normalized EPR decay plots of BzNSN radical anions in the CH_3CN with different electrolyte salts. All solutions contain 20 mM radical and 0.5 M electrolyte salt, charged at 100% SOC, 3C. Dash line indicates half lifetime.

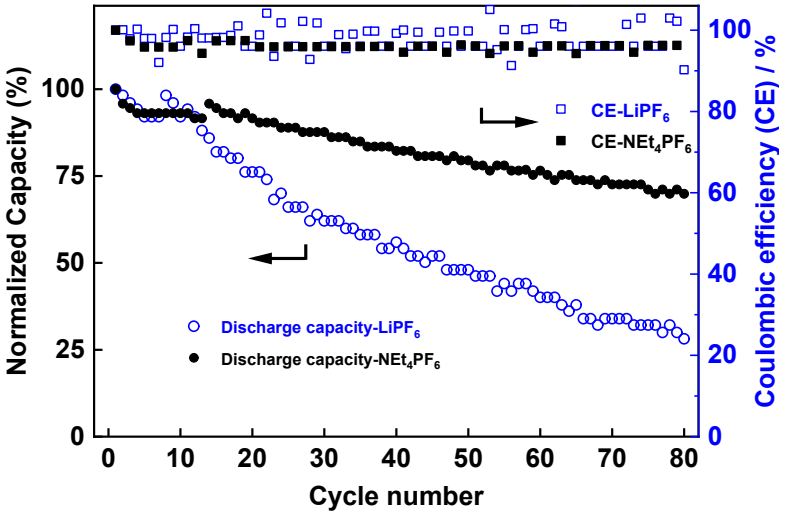

Figure 8. The capacity retention and coulombic efficiency (CE) profiles of H-cell cycling of BzNSN (5 mM) in CH_3CN supporting electrolytes containing various salts (0.5 M) such as $LiPF_6$ and NEt_4PF_6.

For redoxmers, the redox potentials often affect their electrochemical stability. For instance, by derivatizing BzNSN with various electron-donating/withdrawing substitutions, the redox potentials can be tuned in a predictable way as the electron-withdrawing effect decreases the potentials while donating effect increases. More importantly, a linear correlation between the

logarithm of the lifetime of the radical anions and the redox potentials of the corresponding substituted BzNSNs was observed, indicating the kinetic stability is strongly dependent on the thermodynamic measure of the redox potentials.[23] The lifetime of charged BzNSN decreases exponentially as the redox potential becomes more negative. This phenomenon has been observed in many flow battery chemistries, which poses a peculiar challenge for designing high energy density flow batteries. However, the solvating effect seems to provide another handle to tune the redox potential without taxing the electrochemical stability. To characterize the electrochemical stability, BzNSN was charged to 100% state of charge (SOC) in various supporting electrolytes, and the resultant samples were monitored using EPR. As shown in Figure 7, the integrated intensity from the EPR was used to detect the stability of the radical cations. While the potential of BzNSN in LiTFSI electrolyte is the highest among the four electrolytes, the EPR half-life time is not the longest. Surprisingly, as the redox potential decreases, except for the Na^+ electrolyte, the EPR half-life time increases. Especially in NEt_4^+ electrolyte, the radical anion of BzNSN was so stable that no obvious decay was observed over the detection time, indicating extraordinary stability. It is the first time that we observed an anolyte molecule that affords higher stability and lower redox potential at the same time.

The unexpected stability of BzNSN from the less coordinating electrolytes was further evaluated in H-cell cycling. 5 mM BzNSN in various supporting electrolytes were cycled symmetrically in H-cells (details can be found in the experimental section). As shown in Figure 8, the cycling performance of BzNSN is far more stable in the NEt_4PF_6 electrolyte compared to the $LiPF_6$ electrolyte, further confirming that the less coordinating NEt_4^+ may help to stabilize the charged species during cycling.

3. Conclusion

Solvation behavior of a highly stable anolyte molecule, 2,13,-benzothiadiazole (BzNSN), was systematically investigated in various supporting electrolytes. Cyclic voltammetry experiments revealed that the choice of cation in the supporting electrolyte salts had a major impact on the electrochemical properties, such as the redox potentials. Li^+ cations had a much more significant impact compared to NEt_4^+ cations as evidenced by the greater redox potential shift in concentration experiments, implying stronger coordination between Li^+ and BzNSN. This trend was further supported by cyclic voltammetry with electrolytes containing Na^+ and K^+ cations. As the size of cations increased from Li^+ to Na^+, K^+, and bulky NEt_4^+, the redox potential of BzNSN decreased gradually. MD and DFT simulation were utilized to understand

the coordination behavior and explain the redox potential shifts. RDF plots revealed that smaller cations, like Li^+, are closer to the charged BzNSN when coordinated, implying stronger coordination. The larger cations, like K^+ and NEt_4^+, are farther away from the charged BzNSN, therefore bearing weak or negligible coordination. In addition, two cations are more likely to coordinate with one BzNSN molecule. Based on the optimized geometry of the coordinated BzNSN, the redox potentials can be calculated, which are consistent with the experimental results. It is therefore believed that the strong coordination from smaller cations may stabilize the radical anion of BzNSN, affording a more positive redox potential.

EPR kinetics of the charged BzNSN in various supporting electrolytes were also investigated. Surprisingly, the lower redox potential solutions containing the large K^+ and NEt_4^+ cations had much longer half-lives, which does not follow the common thermodynamic-kinetic relationship previously observed.[23] To increase the energy density of RFBs, anolyte redoxmers need to have low redox potentials so that the overall cell voltage can be pushed higher. However, lower potentials also mean higher energy, faster decay kinetics, and shorter calendar lives of the charged species. [23] Many efforts have been conducted to overcome this seemingly inevitable dilemma, and only a handful of successes have been seen.[25] The unexpected result from this study may provide a solvation handle that can overcome the thermodynamic/kinetic constrain for designing high-energy redoxmers. This is the first demonstration of using solvation means to tune an anolyte molecule with a synergetic improvement of two often conflicting properties: a lower redox potential AND a higher stability of the charged radical anion, both of which are desirable for building a high-performance NRFB. While this concurrent improvement still requires further understanding, especially regarding the improved stability, this study represents one unique approach using solvation handle to construct a high energy density and long-lasting NRFB and may serve as a guidance for further development of such systems.

4. Experimental Section

***Materials**:* Lithium bis (trifluoromethane) sulfonimide (LiTFSI, 99.95% trace metal basis), lithium hexafluorophosphate ($LiPF_6$, >99% for electrochemical analysis), tetraethylammonium hexafluorophosphate (NEt_4PF_6, >99% for electrochemical analysis) and acetonitrile (CH_3CN, electronic grade, 99.999% trace metal basis) were purchased from Sigma-Aldrich. Sodium bis(trifluoromethane) sulfonimide (NaTFSI, 99.9%), potassium bis(trifluoromethane) sulfonimide (KTFSI, 99.5%), and tetraethylammonium bis(trifluoromethane) sulfonimide (NEt_4TFSI, >98%) were ordered from Ionic Liquids Technologies (Heilbronn, Germany).

Lithium bis(fluorosulfonyl)imide (LiFSI, 99.9%) was obtained from Nippon Shokubai Co Ltd. All salts were dried at 120 °C under high vacuum overnight before use. The CH_3CN was dried over 3 Å molecular sieves for two days prior to use. 2,1,3-Benzothiadiazole (BzNSN, >99%) was purchased from Tokyo Chemical Industry Co., Ltd. (TCI) and used as received. All chemicals were stored in an argon-filled glovebox (O_2< 5 ppm, H_2O< 0.6 ppm).

Electrochemical and kinetic measurements : Cyclic voltammograms were collected in a three-electrode configuration with iR compensation for 10 mM BzNSN solution at different sweep rates from 10 to 100 mV/s (CHI760D electrochemical workstation CH Instruments, TX). The various Li-based salts (LiTFSI, $LiPF_6$ and LiFSI) and NEt_4-based (NEt_4TFSI and NEt_4PF_6) salts were selected as supporting electrolytes, and CH_3CN was used as the solvent. A glassy carbon disk electrode (CHI 104, the diameter of 3 mm), a Pt wire (CHI 115), and silver/silver nitrate ($Ag/AgNO_3$, 10 mM in CH_3CN) were used as working electrode, counter electrode, and reference electrode, respectively. All measured redox potentials have been verified using ferrocene as an internal reference. Galvanostatic electrolysis was performed in a borosilicate H-cell, which was separated by ceramic porous membrane (P5, Adams and Chittenden) and filled with 4.0 mL of electrolyte in each half-cell. To minimize concentration polarization, the electrolyte in each chamber was stirred (~700 rpm/min). Reticulated vitreous carbon (45 PPI, ERG Aerospace Corporation) was used as working and counter electrode in the two chambers. The electrolytes containing 20 mM BzNSN and 0.5 M supporting salt in CH_3CN were cycled between -2.0 V vs Ag/Ag^+ and -1.2 V vs Ag/Ag^+ at a rate of 3C. After the first cycle, the solvent breakdown products of oxidation were removed from the counter electrode chamber to avoid contamination and replaced with a fresh solution. In this "symmetric" cell, the molecule is reduced in one compartment while the radical anion is oxidized in the second comparment. For kinetic studies, we used the same setup to completely reduce BzNSN and used electron paramagnetic spectroscopy (EPR) to observe the decay of the radical anions *in situ* to study their kinetics. The first-derivative EPR spectra were collected at 25 ^oC using a Bruker ESP300E X-band spectrometer operating at 9.43 GHz; 100 kHz field modulation at $2x10^{-5}$ T.

Classical MD systems and methods

The classical MD simulation system was composed of charged/neutral BzNSN, supporting salt (e.g., LiTFSI, NaTFSI, KTFSI, NEtTFSI), and solvent (i.e., CH_3CN) (see Table 1). The initial configuration of the simulation system was packed using the Packmol code.[35] The

simulation box is periodic in all three directions. The force fields of the system were built based on the OPLS-aa force field.[36, 37] The atomic charge distribution for the changed and neutral BzNSN and NEt^+ ions was computed by fitting the molecular electrostatic potential using a grid-based method at the HF/6-31G(d,p) method using the Gaussian 09 program.[38] Then the atomic partial charges are scaled by 0.8 as a compensation of the charge transfer and polarization effect.[39, 40]

The classical MD simulations were performed using the GROMACS code[41] with a 2 fs time step. First, a 20 ns equilibrium simulation was conducted under the NPT ensemble. The concentrations of the BzNSN and salt were summarized in Table 2. Then, a 20 ns production run was performed under the NVT ensemble with the relaxed volume. The non-electrostatic interactions were computed by direct summation with a cutoff length of 1.2 nm. The electrostatic interactions were computed using the particle mesh Ewald (PME) method.[42] The real space cutoff and fast Fourier transform spacing were set to 1.2 and 0.12 nm, respectively. The Nose-Hoover thermostat was used to stabilize the system temperature at 300 K with a time constant of 1 ps.[43, 44] The Parrinello-Rahman barostat was used to maintain the system pressure at 1 atm with a time constant of 10 ps.[45, 46] The last 10 ns trajectory in the production run is used for the following analysis.

Table 2. Setup of the MD systems studied in this work

System Name	BzNSN no.	Cation no.$^+$	TFSI no.	Acetonitrile no.	BzNSN *c** (mM)	Salt *c** (M)
Li	1	51/50	50	1910	8.3	0.41
Na	1	51/50	50	1880	8.4	0.42
K	1	51/50	50	1880	8.3	0.42
NEt	1	51/50	50	1700	8.7	0.43

$^+$The number of cations is 51 or 50 for the system with charged or neutral BzNSN **c* is the molar concentration

Ab initio MD systems and methods

Ab initio MD systems is composed of 1 $BzNSN^{\bullet-}$ ion, 6 $TFSI^-$ ion, 7 Li^+ ion, and 21 CH_3CN molecules. The simulation box size (1.4841 Å) was calculated based on the experimental densities of 3 M LiTFSI in CH_3CN. The *ab initio* MD was used to validate the classical force field. The choice of the high salt and BzNSN concentrations is due to the limitation of computational efficiency. The system was firstly relaxed using classical MD, followed by the

AIMD simulation. The *ab initio* MD simulations were carried out using the VASP code.[47, 48] The projector augmented waves (PAW) method was used to compute the interatomic forces with the Perdew-Burke-Ernzerhof (PBE) generalized gradient approximation for the exchange-correlation energy.[49, 50] The plane waves energy cutoff was set as 600 eV, and the Brillouin zone was sampled at the Γ-point.[51] A 30 ps trajectory was produced for each system under NVT ensemble for the analysis.

DFT calculations

The geometries of the $BzNSN^{\bullet-}$ and two cations in the first solvation shell extracted from the MD simulation were optimized at the DFT level with the B3LYP/6-311+G(2d,p) method using the Gaussian 09 program.[38] The solvation effect is considered by the CPCM model with a dielectric constant of 35.688 to mimic the CH_3CN solvent. For the neutral BzNSN, the geometry optimization process starts from the molecular geometry of the charged system. The redox potentials of the $BzNSN^{\bullet-}$ with the coordinated cations are computed through the free energy changes for the reduction/oxidation processes (see Eq. 1).[52]

$$E = \frac{-(\Delta G_{charged} - \Delta G_{neutral})}{nF} - 4.44 - 0.8 \qquad (1)$$

Where, $\Delta G_{charged}$ and $\Delta G_{neutral}$ are the free energy of charged and neutral redoxmer with coordinated cations, respectively. *n* is the number of electrons involved in the redox reaction and F is Faraday constant. The constant -4.44 and -0.8 V represents the absolute H_2 potential and standard electrode potentials in aqueous Ag^+ solution at 25 °C.

Acknowledgements

This research was financially supported by the Joint Center for Energy Storage Research (JCESR), an Energy Innovation Hub funded by the U.S. Department of Energy, Office of Science, and Basic Energy Sciences. The submitted manuscript has been created by UChicago Argonne, LLC, Operator of Argonne National Laboratory ("Argonne"). Argonne, a U.S. Department of Energy Office of Science laboratory, is operated under Contract No. DE-AC02-06CH11357. This work is also supported by Laboratory Directed Research and Development (LDRD) funding from Argonne National Laboratory, provided by the Director, Office of Science, of the U.S. Department of Energy under Contract No. DE-AC02-06CH11357. Yuyue Zhao and Zhou Yu contributed equally to this work

Reference:

1. B. Dunn, H. Kamath and J.-M. Tarascon, *Electrical Energy Storage for the Grid: A Battery of Choices*, *Science*, 2011, **334**, 928-935.
2. Z. Yang, J. Zhang, M. C. W. Kintner-Meyer, X. Lu, D. Choi, J. P. Lemmon and J. Liu, *Electrochemical Energy Storage for Green Grid*, *Chemical Reviews*, 2011, **111**, 3577-3613.
3. W. Wang, Q. T. Luo, B. Li, X. L. Wei, L. Y. Li and Z. G. Yang, *Recent Progress in Redox Flow Battery Research and Development*, *Advanced Functional Materials*, 2013, **23**, 970-986.
4. G. L. Soloveichik, *Flow Batteries: Current Status and Trends*, *Chemical Reviews*, 2015, **115**, 11533-11558.
5. J. Noack, N. Roznyatovskaya, T. Herr and P. Fischer, *The Chemistry of Redox-Flow Batteries*, *Angewandte Chemie-International Edition*, 2015, **54**, 9775-9808.
6. A. Weber, M. Mench, J. Meyers, P. Ross, J. Gostick and Q. Liu, *Redox flow batteries: a review*, *Journal of Applied Electrochemistry*, 2011, **41**, 1137-1164.
7. P. Leung, X. H. Li, C. P. de Leon, L. Berlouis, C. T. J. Low and F. C. Walsh, *Progress in redox flow batteries, remaining challenges and their applications in energy storage*, *RSC Advances*, 2012, **2**, 10125-10156.
8. M. Skyllas-Kazacos, M. H. Chakrabarti, S. A. Hajimolana, F. S. Mjalli and M. Saleem, *Progress in Flow Battery Research and Development*, *Journal of the Electrochemical Society*, 2011, **158**, R55-R79.
9. H. N. Chen and Y. C. Lu, *A high-energy-density multiple redox semi-solid-liquid flow battery*, *Advanced Energy Materials*, 2016, **6**, 1502183.
10. H. D. Pratt, N. S. Hudak, X. K. Fang and T. M. Anderson, *A polyoxometalate flow battery*, *Journal of Power Sources*, 2013, **236**, 259-264.
11. G. Nagarjuna, J. S. Hui, K. J. Cheng, T. Lichtenstein, M. Shen, J. S. Moore and J. Rodriguez-Lopez, *Impact of Redox-Active Polymer Molecular Weight on the Electrochemical Properties and Transport Across Porous Separators in Nonaqueous Solvents*, *Journal of the American Chemical Society*, 2014, **136**, 16309-16316.
12. E. C. Montoto, G. Nagarjuna, J. S. Hui, M. Burgess, N. M. Sekerak, K. Hernandez-Burgos, T. S. Wei, M. Kneer, J. Grolman, K. J. Cheng, J. A. Lewis, J. S. Moore and J. Rodriguez-Lopez, *Redox Active Colloids as Discrete Energy Storage Carriers*, *Journal of the American Chemical Society*, 2016, **138**, 13230-13237.
13. C. S. Sevov, S. L. Fisher, L. T. Thompson and M. S. Sanford, *Mechanism-Based Development of a Low-Potential, Soluble, and Cyclable Multielectron Anolyte for Nonaqueous Redox Flow Batteries*, *Journal of the American Chemical Society*, 2016, **138**, 15378-15384.
14. Y. Ding, Y. Zhao, Y. Li, J. B. Goodenough and G. Yu, *A high-performance all-metallocene-based, non-aqueous redox flow battery*, *Energy & Environmental Science*, 2017.
15. M. Duduta, B. Ho, V. C. Wood, P. Limthongkul, V. E. Brunini, W. C. Carter and Y. M. Chiang, *Semi-Solid Lithium Rechargeable Flow Battery*, *Advanced Energy Materials*, 2011, **1**, 511-516.
16. F. Y. Fan, W. H. Woodford, Z. Li, N. Baram, K. C. Smith, A. Helal, G. H. McKinley, W. C. Carter and Y. M. Chiang, *Polysulfide Flow Batteries Enabled by Percolating Nanoscale Conductor Networks*, *Nano Letters*, 2014, **14**, 2210-2218.
17. C. Jia, F. P. Pan, Y. G. Zhu, Q. Huang, L. Lu and Q. Wang, *High–energy density nonaqueous all redox flow lithium battery enabled with a polymeric membrane*, *Science Advances*, 2015, **1**, e1500886.

18. Q. Z. Huang, J. Yang, C. B. Ng, C. Jia and Q. Wang, *A redox flow lithium battery based on the redox targeting reactions between LiFePO4 and iodide*, *Energy & Environmental Science*, 2016, **9**, 917-921.
19. K. Gong, Q. Fang, S. Gu, S. F. Y. Li and Y. Yan, *Nonaqueous redox-flow batteries: organic solvents, supporting electrolytes, and redox pairs*, *Energy & Environmental Science*, 2015, **8**, 3515-3530.
20. J. Winsberg, T. Hagemann, T. Janoschka, M. D. Hager and U. S. Schubert, *Redox-Flow Batteries: From Metals to Organic Redox-Active Materials*, *Angewandte Chemie-International Edition*, 2017, **56**, 686 –711.
21. M. Park, J. Ryu, W. Wang and J. Cho, *Material design and engineering of next-generation flow-battery technologies*, *Nat. Rev. Mater.*, 2016, Article number: 16080.
22. W. Duan, J. Huang, J. A. Kowalski, I. A. Shkrob, M. Vijayakumar, E. Walter, B. Pan, Z. Yang, J. D. Milshtein, B. Li, C. Liao, Z. Zhang, W. Wang, J. Liu, J. S. Moore, F. R. Brushett, L. Zhang and X. Wei, *"Wine-Dark Sea" in an Organic Flow Battery: Storing Negative Charge in 2,1,3-Benzothiadiazole Radicals Leads to Improved Cyclability*, *ACS Energy Letters*, 2017, **2**, 1156-1161.
23. J. Huang, W. Duan, J. Zhang, I. A. Shkrob, R. S. Assary, B. Pan, C. Liao, Z. Zhang, X. Wei and L. Zhang, *Substituted thiadiazoles as energy-rich anolytes for nonaqueous redox flow cells*, *Journal of Materials Chemistry A*, 2018, **6**, 6251-6254.
24. J. Huang, B. Pan, W. Duan, X. Wei, R. S. Assary, L. Su, F. R. Brushett, L. Cheng, C. Liao, M. S. Ferrandon, W. Wang, Z. Zhang, A. K. Burrell, L. A. Curtiss, I. A. Shkrob, J. S. Moore and L. Zhang, *The lightest organic radical cation for charge storage in redox flow batteries*, *Scientific Reports*, 2016, **6**, 32102.
25. J. Zhang, Z. Yang, I. A. Shkrob, R. S. Assary, S. o. Tung, B. Silcox, W. Duan, J. Zhang, C. C. Su, B. Hu, B. Pan, C. Liao, Z. Zhang, W. Wang, L. A. Curtiss, L. T. Thompson, X. Wei and L. Zhang, *Annulated Dialkoxybenzenes as Catholyte Materials for Non-aqueous Redox Flow Batteries: Achieving High Chemical Stability through Bicyclic Substitution*, *Advanced Energy Materials*, 2017, **7**, 1701272-n/a.
26. J. Zhang, J. Huang, L. A. Robertson, R. S. Assary, I. A. Shkrob and L. Zhang, *Elucidating Factors Controlling Long-Term Stability of Radical Anions for Negative Charge Storage in Nonaqueous Redox Flow Batteries*, *The Journal of Physical Chemistry C*, 2018, **122**, 8116-8127.
27. K. H. Hendriks, C. S. Sevov, M. E. Cook and M. S. Sanford, *Multielectron Cycling of a Low-Potential Anolyte in Alkali Metal Electrolytes for Nonaqueous Redox Flow Batteries*, *ACS Energy Letters*, 2017, **2**, 2430-2435.
28. R. Yang, Y. Zhang, K. Takechi and E. J. Maginn, *Investigation of the Relationship between Solvation Structure and Battery Performance in Highly Concentrated Aqueous Nitroxy Radical Catholyte*, *The Journal of Physical Chemistry C*, 2018, **122**, 13815-13826.
29. L. Li, S. Kim, W. Wang, M. Vijayakumar, Z. Nie, B. Chen, J. Zhang, G. Xia, J. Hu, G. Graff, J. Liu and Z. Yang, *A Stable Vanadium Redox-Flow Battery with High Energy Density for Large-Scale Energy Storage*, 2011, **1**, 394-400.
30. M. Vijayakumar, L. Li, G. Graff, J. Liu, H. Zhang, Z. Yang and J. Z. Hu, *Towards understanding the poor thermal stability of V5+ electrolyte solution in Vanadium Redox Flow Batteries*, *Journal of Power Sources*, 2011, **196**, 3669-3672.
31. G. H. A. A. Akhil, A. B. Currier, B. C. Kaun, D. M. Rastler, S. B. Chen, A. L. Cotter, D. T. Bradshaw, W. D. Gauntlett, , *DOE/EPRI 2013 Electricity Storage Handbook in Collaboration with NRECA, SANDIA REPORT, SAND2013-5131,* , 2013.
32. B. Li, Z. Nie, M. Vijayakumar, G. Li, J. Liu, V. Sprenkle and W. Wang, *Ambipolar zinc-polyiodide electrolyte for a high-energy density aqueous redox flow battery*, *Nature Communications*, 2015, **6**, 6303.

33. C. Xie, H. Zhang, W. Xu, W. Wang and X. Li, *A Long Cycle Life, Self-Healing Zinc–Iodine Flow Battery with High Power Density*, 2018, **57**, 11171-11176.
34. J. N. Israelachvili, *Intermolecular and Surface Forces*, 2011.
35. L. Martínez, R. Andrade, E. G. Birgin and J. M. Martínez, *PACKMOL: a package for building initial configurations for molecular dynamics simulations*, *Journal of computational chemistry*, 2009, **30**, 2157-2164.
36. W. L. Jorgensen, D. S. Maxwell and J. Tirado-Rives, *Development and testing of the OPLS all-atom force field on conformational energetics and properties of organic liquids*, *Journal of the American Chemical Society*, 1996, **118**, 11225-11236.
37. B. Doherty, X. Zhong, S. Gathiaka, B. Li and O. Acevedo, *Revisiting OPLS force field parameters for ionic liquid simulations*, *Journal of chemical theory and computation*, 2017, **13**, 6131-6145.
38. M. Frisch, G. Trucks, H. Schlegel, G. Scuseria, M. Robb, J. Cheeseman, G. Scalmani, V. Barone, B. Mennucci and G. Petersson, *Gaussian 09, version D. 01*, *Gaussian, Wallingford*, 2009.
39. C. Schröder, *Comparing reduced partial charge models with polarizable simulations of ionic liquids*, *Physical Chemistry Chemical Physics*, 2012, **14**, 3089-3102.
40. D. Marrocchelli, M. Salanne, P. A. Madden, C. Simon and P. Turq, *The construction of a reliable potential for GeO2 from first principles*, *Molecular Physics*, 2009, **107**, 443-452.
41. B. Hess, C. Kutzner, D. Van Der Spoel and E. Lindahl, *GROMACS 4: algorithms for highly efficient, load-balanced, and scalable molecular simulation*, *Journal of chemical theory and computation*, 2008, **4**, 435-447.
42. T. Darden, D. York and L. Pedersen, *Particle mesh Ewald: An N· log (N) method for Ewald sums in large systems*, *The Journal of chemical physics*, 1993, **98**, 10089-10092.
43. S. Nosé, *A molecular dynamics method for simulations in the canonical ensemble*, *Molecular physics*, 1984, **52**, 255-268.
44. W. G. Hoover, *Canonical dynamics: Equilibrium phase-space distributions*, *Physical review A*, 1985, **31**, 1695.
45. M. Parrinello and A. Rahman, *Polymorphic transitions in single crystals: A new molecular dynamics method*, *Journal of Applied physics*, 1981, **52**, 7182-7190.
46. S. Nosé and M. Klein, *Constant pressure molecular dynamics for molecular systems*, *Molecular Physics*, 1983, **50**, 1055-1076.
47. G. Kresse and J. Hafner, *Ab initio molecular-dynamics simulation of the liquid-metal–amorphous-semiconductor transition in germanium*, *Physical review B*, 1994, **49**, 14251.
48. G. Kresse and J. Furthmüller, *Efficiency of ab-initio total energy calculations for metals and semiconductors using a plane-wave basis set*, *Computational materials science*, 1996, **6**, 15-50.
49. G. Kresse and D. Joubert, *From ultrasoft pseudopotentials to the projector augmented-wave method*, *Physical review B*, 1999, **59**, 1758.
50. J. P. Perdew, K. Burke and M. Ernzerhof, *Generalized gradient approximation made simple*, *Physical review letters*, 1996, **77**, 3865.
51. H. J. Monkhorst and J. D. Pack, *Special points for Brillouin-zone integrations*, *Physical review B*, 1976, **13**, 5188.
52. L. Cheng, R. S. Assary, X. Qu, A. Jain, S. P. Ong, N. N. Rajput, K. Persson and L. A. Curtiss, *Accelerating electrolyte discovery for energy storage with high-throughput screening*, *The journal of physical chemistry letters*, 2015, **6**, 283-291.